Review

Field Emission from Carbon Nanostructures

Filippo Giubileo [1,*] **, Antonio Di Bartolomeo** [1,2] **, Laura Iemmo** [1,2] **, Giuseppe Luongo** [1,2] **and Francesca Urban** [1,2]

1   CNR-SPIN Salerno, via Giovanni Paolo II, n. 132, 84084 Fisciano, Italy
2   Dipartimento di Fisica "E.R. Caianiello", Università di Salerno, via Giovanni Paolo II, n. 132, 84084 Fisciano, Italy; adibartolomeo@unisa.it (A.D.B.); liemmo@unisa.it (L.I.); giluongo@unisa.it (G.L.); furban@unisa.it (F.U.)
*   Correspondence: filippo.giubileo@spin.cnr.it; Tel.: +39-089-969329

check for updates

Abstract: Field emission electron sources in vacuum electronics are largely considered to achieve faster response, higher efficiency and lower energy consumption in comparison with conventional thermionic emitters. Carbon nanotubes had a leading role in renewing attention to field emission technologies in the early 1990s, due to their exceptional electron emitting properties enabled by their large aspect ratio, high electrical conductivity, and thermal and chemical stability. In the last decade, the search for improved emitters has been extended to several carbon nanostructures, comprising carbon nanotubes, either individual or films, diamond structures, graphitic materials, graphene, etc. Here, we review the main results in the development of carbon-based field emitters.

Keywords: carbon nanostructures; field emission; Fowler-Nordheim; vacuum electronics

1. Introduction

Several technological applications need controlled electron sources, examples are X-ray sources [1], flat panel displays [2,3], electron microscopy/lithography [4], and microwave vacuum electronic devices [5]. One of the most common techniques for generating an electron beam is to emit electrons from metals by thermionic effect, in which a metallic emitter is heated at temperatures typically above 1000 °C so that electrons in the conduction band gain enough energy to overcome the work function of the emitter. However, the main drawbacks of thermionic emission are the high energy consumption, the wide energy spectrum of the emitted electrons and the material degradation caused by the high operating temperature. A different approach is that of the "cold cathodes", which operate at room temperature. Electrons are extracted from the surface of a metal or a semiconductor by an electric field (field emission, FE) through quantum mechanical tunneling. This process, which typically requires a high electric field (10^7–10^8 V/cm) [6], creates high current density with thinner energy distribution of the emitted electrons [7,8]. Moreover, cold cathodes provide very stable emission over time, and can be easily and advantageously miniaturized.

In this review, we focus on the field emission properties of various carbon nanostructures. In particular, after a brief introduction to the field emission phenomenon, we examine the different experimental setups used for FE characterization as well as the technology in which FE has been traditionally exploited. We turn then to the different carbon allotropes, and we review the main results concerning field emission from carbon nanotube (CNT) films, individual CNTs, diamond and related structures, and finally graphene.

Field Emission

In order to escape from a metal surface, electrons need sufficient energy to overcome the potential barrier at the metal-vacuum interface, i.e., the potential difference between the Fermi level of the metal

and the vacuum. Such energy is known as the metal work-function and denoted by ϕ in the following. It is a material property and has a crucial role in its electron emission capability. Figure 1 shows the effective potential on an electron at a distance x from the emitting surface when an electric field E is applied perpendicularly to the surface. The applied electric field E modifies the potential barrier that becomes thinner (triangular) and the effective barrier height is lowered. Typically, appreciable tunneling is expected for an applied electric field above 3×10^7 V/cm [9]. The width of the tunneling barrier ranges from 4.5 nm at 3×10^7 V/cm to 0.5 nm at 3×10^8 V/cm for a metal surface having a $\phi \approx 4.5$ eV.

(a) (b) (c)
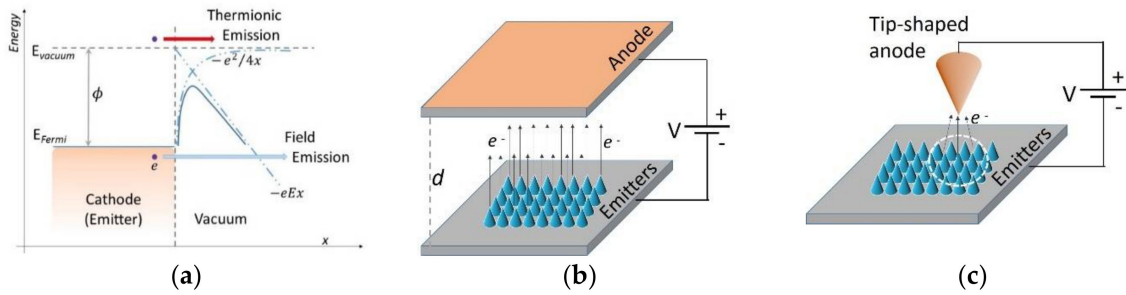
Figure 1. (**a**) Potential energy of the electron as function of the distance x from the metal-vacuum interface. The barrier for electron field emission is thinned and lowered by the electric field and the image force, which add to ϕ the position-dependent terms $-eEx$ and $-e^2/4x$, respectively. Experimental setup for field emission measurements in the (**b**) parallel plate and (**c**) tip configuration for average and local characterization, respectively.

From a theoretical viewpoint, the FE is described by the Fowler-Nordheim (F-N) theory [10] based on a simplified one-dimensional free electron model and Wentzel-Kramers-Brillouin (WKB) approximation to calculate tunneling probability for a planar metallic emitter [11]. According to this model, the FE current density J at 0 K depends on the local electric field E_{local} and on the work function ϕ as

$$J = a \frac{E_{local}^2}{\phi} \cdot exp\left(-b \frac{\phi^{3/2}}{E_{local}} \right) \tag{1}$$

where $a = 1.54 \times 10^{-6}$ A V^{-2} eV and $b = 6.83 \times 10^7$ cm^{-1} V eV$^{-3/2}$ are constants. The macroscopic electric field E and the local field are related by the field enhancement factor β as $E_{local} = \beta \cdot E$, to take into account the emitter geometry, when the emitter is not flat. For flat surfaces, impractically high macroscopic fields of the order of several kV/μm must be applied in order to switch on emitted density current of the order of few mA/cm^2. On the other hand, tip-shaping of the emitter can result in a high enhancement factor, that is a high local electric field, and trigger field emission under a very low macroscopic field. From Equation (1), the FE is favored for materials with low work function. Although the F-N model has been developed for emission under a uniform macroscopic electric field, typical of the parallel plate setup of Figure 1b, it has been demonstrated that it can be satisfactorily applied to more complex geometries, where a non-uniform electric field is generated for example by a tip-shaped anode, as shown in Figure 1c [12,13]. In a more advanced approach, corrections are necessary to consider non-uniform field enhancement factor or work-functions, curved surfaces, non-zero temperature, series resistance, etc. [14,15]. Forbes et al. [16,17] proposed a more accurate model to deal with metallic nanowire large-area field emitters, but the corrections introduced therein do not seem very relevant in the case of carbon nanotubes [18]. More rigorous approaches have been also reported in order to consider either the atomic geometry or electronic structure of the emitters [19–22], including first-principles calculations [23,24]. However, the original F-N formulation is still widely applied by the scientific community to analyze experimental data with good approximation and gain an initial insight into the emission phenomena from new emitters. Examples are recent studies on FE

from nanowires (GaN [25], ZnO [26], GaAs [27]), nanoparticles (In_2O_3 [28], GeSn [29], InP [30]), CNT structures [31–36], two-dimensional materials (graphene [37–39], MoS_2 [40,41]), etc.

Moreover, the comparison between one-dimensional and three-dimensional models for source structures [42] has also confirmed that no relevant differences are expected in describing the field emission characteristics.

2. Field Emission from Carbon Nanostructures

2.1. Field Emission Technology Development

Due to the exponential dependence of the emitted current on the local electric field as well as on the work function (see Equation (1)), small variations of the chemical state of the surface or of the shape of the emitters strongly influence the emission properties. Since the early sixties, a huge effort has been focused on reducing the applied electric field/voltage necessary to enable electron emission. This has been carried out by sharpening the emitter surface thereby profiting from the enhanced field factor at the tip apices. On the other hand, reducing the curvature radius of an emitter apex to obtain higher β, also corresponds to a reduction in the effective emitting area, which limits the maximum current emitted from a single structure. For instance, the current from a single tip can rarely exceed 10^{-4} A (despite high current density being easily obtained). This implies that emitters with a very small curvature radius are suitable when a narrow-spectrum rather than a high-current electron source is required, such as in high-resolution scanning electron microscopy. At the same time, materials for FE should have high electronic conductivity, high melting points, chemical inertness, and mechanical stiffness.

Mature technology was achieved before the nineties with the development of micro-gated field-emission arrays (FEAs) called Spindt emitters [43], in which large arrays are created by micro-fabrication technology employed in the electronics industry (Figure 2) to be employed for flat panel displays [44,45].
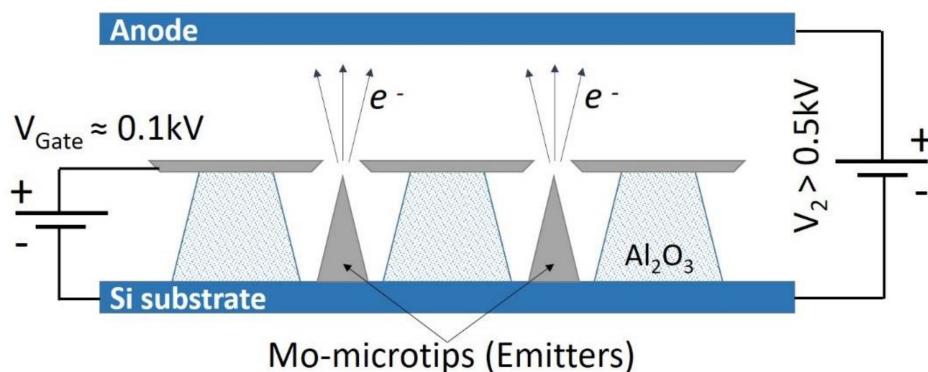

Figure 2. Schematic of Spindt-type emitters.

FEAs are typically fabricated by means of a lithographic process to realize an ordered two-dimensional arrangement of individual molybdenum micrometric conical emitters, in gated configuration, on a Si-substrate. Typically, molybdenum is the material of choice because of its good thermal, mechanical and electrical properties, having $\phi = 4.6$ eV, low resistivity and a high melting point, which allows high currents. The main drawbacks of such a technology are related to the complex and expensive fabrication process, the critical lifetime in vacuum, and the still relatively high operating voltages.

2.2. Carbon Allotropes

In 1991 a great breakthrough in the field of carbon science and technology occurred with the discovery of one-dimensional allotrope of carbon, the so-called carbon nanotubes (CNTs) by Iijima et al. [46]. Nowadays, known carbon allotropes (Figure 3) are diamond, graphite, graphene, fullerene and amorphous carbon. A CNT is a cylinder obtained by rolling up graphene sheets; a single walled nanotube (SWNT) is obtained by a single graphene layer forming a cylinder with a diameter of about 1 nm and length up to few mm [47,48]; a multi-walled nanotube (MWNT) is a set of concentric cylinders with a total diameter up to 100 nm and a length of tens of microns. CNTs properties are strongly dependent on atomic arrangement, diameter and length.
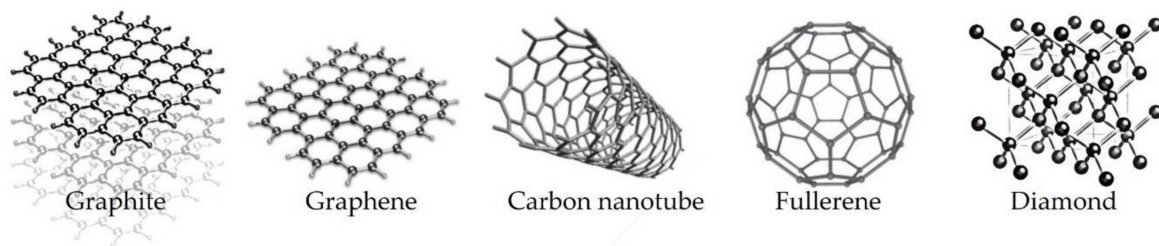
Figure 3. Carbon allotropes: Graphite (3D), Graphene (2D), CNT (1D), Fullerene (0D) and Diamond (3D).

CNTs are being widely studied because of their unique structure and extraordinary properties. The mechanical properties and chemical inertness, associated with structure dependent electronic properties and high aspect ratio make CNTs suitable for several innovative technologies. CNTs have already been applied as field-effect transistors [49–51], memory devices [52], nano-tip for atomic force microscopy [53], hydrogen storage system [54,55], active electrode in supercapacitors [56–58], transparent conductive thin films [59,60], power transmission lines with high current-carrying capacity up to 10^5 A/cm^2 [61], etc.

The application of CNTs as electron field emitters has been widely investigated ever since it was firstly demonstrated in 1995 [62,63]. Indeed, the above recalled properties [64,65] make CNTs excellent emitters, suitable for many applications such as high-resolution electron microscopes as well as electron beam lithography [66,67], X-ray tubes [68,69], and flat panel displays [70,71].

A detailed review of the CNT properties and synthesis methods is out of the scope of this review and this can be found in [72,73].

The high aspect ratio of CNTs is responsible for an extremely large field enhancement factor and provokes very high local electric field intensities around the nanotube apices. Moreover, even in the case of damaging due to arc discharge, the field enhancement factor typically does not result in much modification. The CNT emitters usually maintain high aspect ratios even after arcing or ion bombardment cuts, differently from Spindt-type emitters, for which important flattening occurs at the tips.

2.3. Field Enhancement Factor, β

The field enhancement factor represents a key figure for characterizing the field emitter performance. Typical experimental procedures to get an estimation of *β* rely on the analysis of the current-voltage characteristics (*I*–*V*) by means of the F-N theory. From Equation (1), a linear dependence is expected for the so-called F-N plot, in which $\ln(I/V^2)$ is reported as a function of $1/V$, with the macroscopic electric field far from the nanotube given by the applied voltage *V* divided by the anode-cathode distance, $E = V/d$. Accordingly, *β* can be obtained from the slope *m* of the linear dependence, being $m = b \cdot \varphi^{3/2} \cdot d / \beta$.

Several models have been proposed to study the dependence of *β* on nanotube geometrical properties, i.e., length *l* and radius *r*. The intrinsic field-enhancement factor of a single CNT in the

planar diode configuration can be written [74] as $\beta = 1.2 \cdot \left(2.5 + \frac{l}{r} \right)^{0.9}$. Typical β values in the range of 3×10^4 to 5×10^4 can be obtained in individual CNTs. Vice versa, when dealing with CNT films typical values are in the range of 1×10^3 to 3×10^3 [75]. A calculation of the field enhancement factor in the vicinity of a CNT apex has been also reported by Smith et al. [76], studying the dependence of β on the lateral separation between CNTs, anode-substrate separation d, and on the geometrical parameters (height h and radius r) of the CNTs. They showed that emitted current, calculated in the framework of F-N theory, is reduced if the nanotubes are separated from each other less than twice their height. It has also been shown that when the inter-tube distance (s) becomes $s < h$, the field enhancement factor decreases rapidly for reducing s. The current emission is optimized when inter-tube distance is comparable to h [77].

Moreover, the anode-cathode distance is relevant as well if it is shorter than $3h$. In particular they predicted that the turn-on field, which is the minimum field required to initiate FE, decreases for decreasing cathode-anode distance; however, for distance larger than $3h$, the turn-on field results are constant and independent from the geometry of the electrodes. Wang et al. [78] used a simple model of a floated sphere inside a standard parallel plate configuration to take into account the anode-cathode separation, and showed that $\beta = (h/r + 3.5) + A(h/d)^3$, A being a constant. This implies that turn-on field or voltage can be reduced by decreasing the anode-cathode distance.

2.4. Emission from CNT Films

Field emission devices based on CNTs can deal either with individual CNTs (working as a point electron emitter) or with CNT ensembles realizing (quasi) planar emission cathodes by producing CNT films, patterned arrays, buckypapers, etc. Point emitters are mostly suitable for focused emission in high-resolution applications, while planar cathodes are the preferred choice for devices working with large emission current (for instance, X-ray sources or flat panel displays). Consequently, a large number of experimental and theoretical studies have been devoted to the characterization of CNT films.

FE from CNT films is reviewed in this section, while the next section is dedicated to emission from individual CNTs.

In 1995, the seminal paper by De Heer et al. [63] demonstrated the fabrication of a continuous nanotube film emitter by using a nanopore alumina filter to draw MWCNTs in a colloidal suspension and transferring the obtained film on a teflon coated metal surface [79]. They demonstrated field emission from MWCNTs with current densities as high as 100 mA/cm^2. Alternatively, suspension can be sprayed on heated substrate [80] to obtain a CNT film. A different approach to obtaining CNT films is to disperse CNTs in a non-conducting epoxy [81]. Other methods reported for the fabrication of CNT film include electrophoresis [82], vacuum filtration [59] and screen-printing [83]. Patterned CNT films can be obtained using post deposition techniques [70,84,85] or direct growth by chemical vapor deposition on catalyst patterns. Actually, field emission properties have been reported to be excellent for almost all types of nanotubes, with threshold fields as low as 1 V/µm, recording current densities up to a few A/cm^2 for applied fields below 10 V/µm. A relevant parameter when dealing with films is the emitter density; although CNT density is typically $\sim 10^8$ cm^{-2}, the number of effective emitters for randomly oriented films is generally lower, from $\sim 10^3$ emitters/cm^2 [79,86–88] to $\sim 10^7$ emitters/cm^2 [89]. In order to provide FE performances comparable to conventional molybdenum (Mo) field emitters in realizing flat panel display, CNT films need to have high uniformity with a density of emitters $\sim 10^6$ emitters/cm^2 and a current density capability exceeding 80 µA/cm^2 [90].

The use of Chemical Vapor Deposition (CVD) techniques to directly grow CNT films on a given substrate is widely applied due to the easy production scalability, for either randomly or vertically aligned tubes. For randomly oriented films, the FE properties are similar to coated CNT films. The main purpose of CNT films is represented by their application as large area electron sources as well as field emission displays [91,92]. On the other hand, patterned films can be obtained by means of lithographic techniques to opportunely shape the catalyst deposition. The further advantage of patterning consists

of the opportunity to further reduce pixel size (typically an intrinsic limitation when producing large area sources with un-patterned films). Consequently, films of vertically aligned CNTs have the largest potential for technological applications due to relatively easy production and their high emission capability [93–95]. Since the nineties, a wide variety of CNT films, vertically or randomly oriented, different for density, substrate, single- or multi-walled tubes, have been deeply investigated as field emission devices [96–98]. Unfortunately, the extreme inhomogeneity arising from the composition and morphology of CNT films, even on small areas, caused a wide variation in the reported experimental data regarding the basic characterization parameters, such as the field enhancement factor, and the turn-on field. Indeed, it has been shown that when characterizing large emitting areas by parallel plate technique, emission from a CNT film typically happens from isolated spots [90], i.e., the emission phenomenon is mostly due to a limited subset of emitters.

Therefore, in order to obtain accurate analysis of FE performance from CNT films, it is essential to characterize emitting areas as small as possible. It has been proposed that FE experiments on vertically aligned MWCNTs (Figure 4) could be performed by scanning probe microscopy (STM/AFM), with the probe working as an anode [12,32]. This technique enables accurate characterization of the local field emission behavior, with only a limited number of emitters contributing to the total current. Indeed, the high spatial resolution provided by the piezo-driven positioner used for STM/AFM microscopy technique allows precise control of the tip-sample separation in the submicron region. By taking into account the small curvature radius (below 50 nm) of the probe tip, it has been estimated that the emitted current comes only from a limited circular area, of radius $r \sim d$ when working at separation distances of the order of 1 μm [12]. Moreover, for a correct analysis of the FE I–V characteristics, it is necessary to introduce a further amplification factor, the tip correction factor k_{eff}, due to the tip shaped anode. Accordingly, the slope m of the F-N plot, $\ln\left(\frac{I}{V^2}\right)$ vs. $1/V$, can be reasonably approximated as $m = k_{eff} \cdot b \cdot \phi^{3/2} \cdot d/\beta$. An example of I–V characteristics measured using a Pt–Ti coated cantilever probe as anode and fixing a cathode-anode separation of 1 μm and a pressure of 2×10^{-8} mbar is shown in Figure 4. Electrical conditioning is obtained during the first sweep and it has been explained in terms of a few protruding longer tubes (degraded/destroyed by raising the current density during the first sweep) and/or the effect of desorption of adsorbates. Moreover, it has been demonstrated that the limited area of emission favors very stable FE current, with fluctuations below 10% for more than 72 h also at intensities as high as 10^{-8}–10^{-5} A.
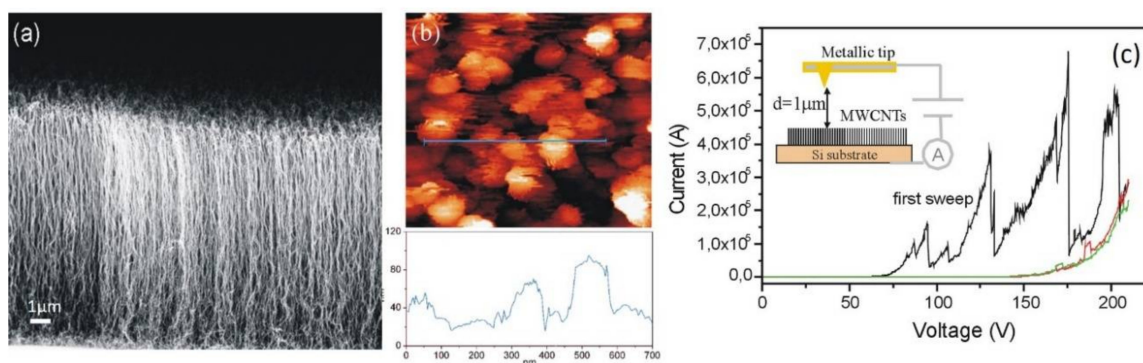
Figure 4. (**a**) SEM image (lateral view) of vertically aligned MWCNTs, grown by catalytic chemical vapor deposition on a silicon substrate with Ni catalyst. (**b**) Scanning Probe Microscopy imaging of 1 μm × 1 μm area of the film surface. Lower plot corresponds to the profile of solid line represented on the image. (**c**) Field emission current versus voltage measured at 1 μm cathode–anode separation and pressure of 2×10^{-8} mbar. After a first sweep from 0 to 200 V the I–V characteristic remains stable for successive sweeps. Adapted with permission from [32], Copyright Elsevier, 2009.

Understanding the physical mechanisms responsible for the emission stability from CNT cathodes, has been widely investigated [99–102], identifying as key factors either the presence of residual gases

and the resistive heating of emitters and the mechanical actions due to high electric fields. Both resistive heating and mechanical actions are related to high fields and high currents and they can be consequently reduced by properly realizing the operational conditions of the FE device. On the contrary, controlling the effects due to a degraded vacuum level, i.e., due to the presence of residual gases, is a much more complicated task. Indeed, residual gases are first of all always present in sealed vacuum devices. Control of the vacuum level between anode and cathode is a crucial parameter, because a degraded vacuum can provoke ionization of the residual gas by the emitted electrons as well as poisoning of the emitting surface, reducing the overall field emission performance. Small variations in the electric field and the work-function may have large effects on the fluctuations of the emitted current due to the exponential behavior of FE. Absorbates on the emitter apex can cause slight modifications of the work-function or of the cap geometry, creating large variations in the emitted current. Such fluctuations disappear almost completely when operating at higher currents. The presence of noble gases as well as H_2 usually provokes an increase in the current fluctuations, but the emission stability can be restored by pumping down the vacuum level. For instance, no degradation was reported on single nanotubes after exposure to Ar and H_2. On the other hand, exposure to oxygen and water causes an irreversible decrease of the emitted current, probably due to reactive sputter etching [103]. A vacuum level of the order of 10^{-9} mbar is suitable for an emission stability of a few percent. Higher pressure also allows FE but with reduced stability. In such a case, it would be useful to reduce the partial pressure of oxygen and water.

Because field emission is strongly influenced by the surface condition of the emitters, it is important to prepare clean emitter surfaces, in order to lower the current fluctuations. Further improvements can be achieved by introducing a ballast resistance in series with the extraction voltage [104]. Kita et al. [105] have investigated the stabilization of the FE current by using a ballast resistance in the range from 1 to 1500 MΩ at an emission current of 1 to 100 μA. They demonstrated excellent stability where the ratio ($\Delta I/I$) of the current fluctuation with respect the absolute current was as small as 0.0018, using 10 MΩ ballast resistance on an average current of about 80 μA.

A different approach to use CNTs in realizing an effective emission cathode (for a flat-panel lighting device) with stable FE as well as low current fluctuations, examines the possibility of properly dispersing CNTs uniformly in a liquid media, thus favoring an extremely homogeneous deposition process. Shimoi et al. [106] successfully produced field emission lighting elements (based on single-walled nanotubes) showing stable electron emission, good luminance, and low power consumption. They chose a low viscosity solvent containing highly crystalline single-walled nanotubes dispersed in a tin-doped indium oxide (ITO) precursor solution (conductive matrix). Also, a non-ionic surfactant was used to favor the dispersion of CNTs. The field emission cathode was obtained by sputtering ITO coating film with single-walled CNTs on glass substrate. Protrusions of the CNTs was obtained by manual scratching. The FE characterization evidenced high electron emission homogeneity, high brightness efficiency (over 70 lm/W) and long emission life-time (estimated above 5000 h).

Current-fluctuation mechanisms of field emitters using metallic single-walled carbon nanotubes with high crystallinity have also been recently discussed [107]. This study is related to the possibility of using field emitters as a cathode electrode in a cathodoluminescence device. The main drawback is due to the use of field emitters that radiate rays whose intensity fluctuates at low frequency, due to FE current fluctuation. Consequently, an important task is having a stable FE output. The authors succeeded in realizing and characterizing cathodoluminescence devices with homogeneous dispersion of metallic single-walled CNTs with high crystallinity. They also developed a theoretical model to study the power spectrum of the current fluctuation considering an inelastic-electron-tunneling model with a Wentzel–Kramers–Brillouin approximation.

2.5. Emission from Individual Nanotubes

The characterization of field emission properties of a single CNT is very important. Typically, electron sources are realized with several emitters and their performances are the result

of statistical averaging. To fully understand the physical mechanisms of electron emission, several studies have been devoted to quantifying the performance of a single CNT as an emitter [13,108–111]. The experiments on individual tubes allows a more accurate characterization of work function, turn-on voltages, current densities, and field enhancement factor as well as monitoring structural modifications [112] and failure mechanisms [102]. Consequently, measurements on individual tubes provide valuable information towards a fundamental understanding of the emission mechanism. Typically, multi-walled CNTs are employed for higher conductance and robustness. The importance of studying the FE behavior of individual tubes is also strictly related to their technological applicability as nano-sized electron sources in high resolution e-beam techniques [113].

I–V characterization of the FE properties of individual multi-walled CNT has often been performed operating with a large cathode-anode separation (several millimeters) to overcome the uncertainty on the cathode-anode separation as well as to obtain a configuration in which the field enhancement factor is only slightly sensitive to the distance. On the other hand, relevant FE applications typically deal with cathode-anode separation below 15 μm to obtain higher fields with lower voltages. At such a distances, the main FE parameters, the field enhancement factor and the turn-on voltage, are very sensitive to distance variations [114]. Field emission properties of a single CNT have been characterized by several groups, reporting emitted currents as high as several tens of microamperes, implementing different measurement setups. A summary of more relevant results available in the literature are collected in Table 1, listing the different parameters, such as CNT dimensions, anode-cathode separation distance, and the extracted FE parameters.

Table 1. Field emission characterization of individual multi-walled CNTs for (CNT apex-anode) distances below 100 μm. Geometrical parameters of the CNT (length and radius), setup configuration being parallel-plate (P-P) or tip-shaped (TIP), field enhancement factor β and turn-on voltage or field are also listed.

CNT Length (μm)	CNT Radius (nm)	CNT Apex-Anode Distance (μm)	Setup	β	Turn-on Voltage (V) or Field (V/μm)	Ref.
3.2	17	0.06–5	TIP	230–460	47–185 V	[115]
5.83	24	10	TIP	208	270 V	[116]
0.5	15–20	10–50	TIP	500–750	60–260 V	[117]
1.5	20	20	P-P	200–500	150–400 V	[118]
3.9	15.8	0.40	P-P	300	100 V	[109]
8	40	1–60	TIP	100–800	40–5 V/μm	[108]
1.3	50	0.29	P-P	140	90 V	[119]
2.1	30	1.4–13.5	P-P	100–700	50–70 V	[120]
5	30	0.8	TIP	110	30 V/μm	[13]

Bonard et al. [115] reported the FE characteristics for individual multi-walled CNT inside a SEM by using a sharp anode for precise measurements in a range of cathode-anode distance from 0.06 to 5 μm. They reported a dependence of the field enhancement factor (up to 460) on such distance in agreement with the Edgcombe and Valdre model [74]. The lowest turn-on voltage was estimated 47 V. Their results also confirmed that only CNTs with the highest field enhancement factor contribute to the emitted current when performing large area measurements.

The electrical properties of individual multi-walled carbon nanotubes grown by plasma enhanced CVD has been also reported [116]. The I–V characteristics have been measured by means of scanning anode field emission system on a vertical array of CNTs separated by 25 μm spacing (allowing to probe the emission from individual tubes). It has been found that field enhancement factor is strongly dependent on the geometry (height/radius) of CNT. To avoid the effects of adsorbates, current annealing (in the micro-ampere range) was performed to favor evaporation of adsorbates/residuals from emitter surface. The experimental data correctly followed F-N theory allowing to extract a field enhancement factor of 208 for 10 μm anode-cathode separation.

Minh et al. [117] developed a selective growth method to realize individual CNTs (using a hot-filament CVD technique with a mixture of C_2H_2 and H_2 gases under a negative substrate biasing) on silicon micro-fabricated tips of about 20 nm diameter. A micro-controlled probe (curvature radius of about 10 μm) was used to perform the FE characterization in a vacuum chamber at a base pressure of 1.7×10^{-4} Pa. The poor vacuum level was recognized as the responsible of current instability. I–V characteristics were measured for a cathode-anode separation from 10 to 50 μm, reporting a turn-on voltage in the range 60–260 V.

She et al. [118] studied the FE properties of individual CNTs grown on silicon tips. The experimental setup, in a SEM chamber with a tungsten probe-tip as anode, allowed precise measurements of CNT morphology as well as geometry of the FE device before and after the events of vacuum breakdown. They recorded un upper limit in emission current density of 10^3 A/m^2. From the comparison of two CNTs of similar length (~1.5 μm) and different diameter (3 nm and 40 nm) they also demonstrated that the vacuum breakdown of the CNTs results in melting of the Si tip.

Interestingly, a study of the field emission properties for individual multi-walled CNTs has been performed inside a transmission electron microscope [119], analyzing the effect of different vacuum levels as well as of contamination conditions. The experimental set up allowed three different geometries for the CNT cathode: a side emission geometry (reporting no emission current); a circular CNT for which only small current (below 5 μA) was recorded; and end-emission geometry (i.e., standard emission from the CNT apex) that resulted in the most favorable configuration for FE. From I–V measurements at a cathode-anode distance of 0.29 μm a field enhancement factor of 140 and a turn-on voltage of about 90 V were reported.

Hii et al. [120] focused on the characterization of field emission from individual CNTs, for cathode-anode separation distances below 15 μm. A wide ranging, systematic study was performed by measuring current-voltage characteristics for several distances in the range 1.4–13.5 μm. From the analysis of experimental data in the framework of F-N theory, it was shown that turn-on voltage as a function of the separation distance d followed an empirical power relation $\sim ad^b$ (with a and b constants), while the field amplification factor followed the relation $\sim d/(d + h)$, where h is the CNT height.

2.6. Field Emission from Diamond and Related Structures

Despite their insulating properties and the expensive cost of both natural and high-pressure synthesis, diamond structures have been identified, since the 1990s, as ideal coating materials for field emission devices due to their negative surface electron affinity, high thermal conductivity and chemical inertness [121–123]. Currently both carbon diamond films (CDF), grown by chemical vapor deposition, or diamond-like carbon films (DLC), produced by ion-beam sputtering deposition of carbon ions, are in use [124]. CDFs can grow on substrates heated at high temperature as poly or single crystalline diamonds with a relatively high surface roughness. Conversely, DLCs have reduced surface roughness and can be obtained on substrates at low temperatures, but generally are characterized by poor thermal stability. Growth conditions have been found to be an important parameter for the field emission properties of these materials, with varying experimental results [125]. Indeed, an extensive experimental study [126] has reported the comparison of FE data obtained on microcrystalline diamond films deposited by hot-filament CVD method and undoped DLC films deposited using radio-frequency CVD technique, showing that surface morphology and emission properties critically depends on the fabrication technique. When imperfect fine-grained diamond films (with the relative high presence of sp^2 carbon phase) are examined, the field emission properties are clearly enhanced (with turn-on fields of about 50 V/μm) with respect to the case of high quality coarse-grained diamond films (characterized by a large amount of the sp^3 phase and a turn-on field of about 140 V/μm). To explain the mechanism of field emission from CVD diamond films, various models have been reported, focusing principally on the negative surface electron affinity [127], on the presence of grain boundaries [128,129], or on the presence of small protuberances [129,130]. The electron affinity (i.e., the energy difference between the

vacuum level and the conduction band minimum in a semiconductor) is typically few eV (positive electron affinity) and it represents the potential barriers that an electron (raised from the valence band to the minimum of conduction band by an excitation) encounters to leave the sample towards the vacuum. On the other hand, in the case of negative electron affinity, the electron at the bottom of the conduction band is free to leave the surface of the material. It has been suggested [67] that negative electron affinity alone cannot completely explain the electron emission from diamond and DLC films. It is now accepted that a pure diamond surface has a small positive electron affinity (~+0.38 eV) [131] that can become negative in the presence of defects or hydrogen terminations. A schematic of the energy band diagram for a clean diamond surface (with positive electron affinity) and for hydrogenated diamond surface (with negative electron affinity) is shown in Figure 5.
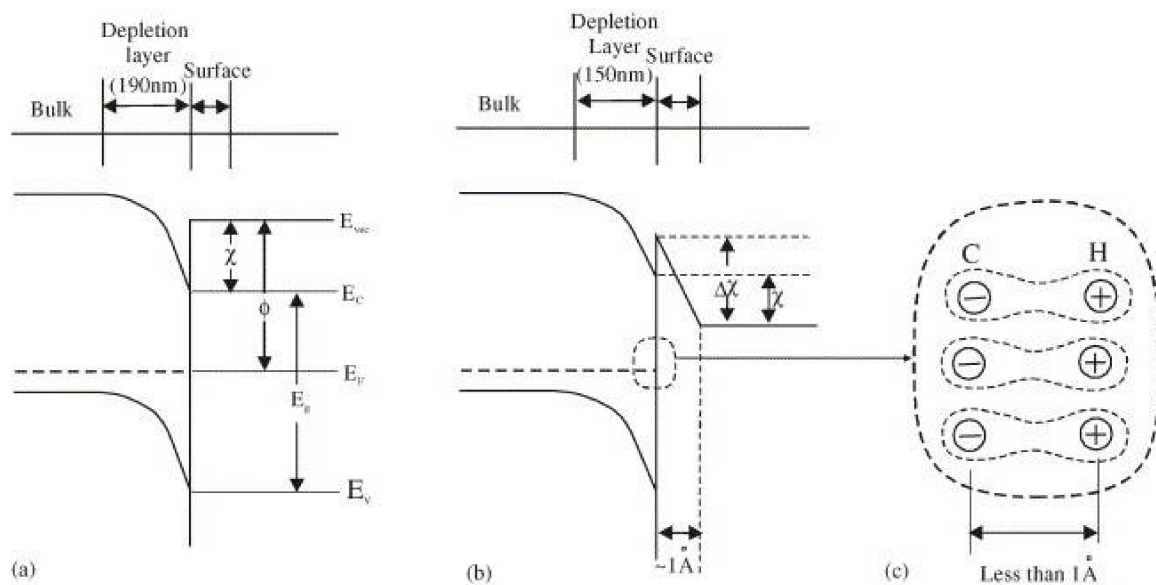
Figure 5. (**a**) Schematic of the energy band diagram for a clean diamond surface with a positive electron affinity. (**b**) Schematic of the energy band diagram of a hydrogenated diamond surface with negative electron affinity. (**c**) Possible atomic arrangement of dipole layer on the hydrogenated diamond surface. The mentioned "surfaces" refer to the single crystalline type IIb diamond. Image reproduced with permission from [67], Copyright Elsevier, 2005.

Low field emission from DLC films has been the subject of several theoretical studies, considering the role of hot electron injection [132], dielectric breakdown [133], tunneling [134], tip emission [135], and defects [136]. It has been shown that low field emission is systematically measured when carbon materials have sp^2 bonds. Graphitic phases, often present in CVD diamond films [137] and in diamond/sp^2-bonded carbon nanocomposites [138], are a crucial ingredient for field emission. Karabutov et al. [139] analyzed the FE properties for different diamond/sp^2-bonded carbon nanostructures including CVD diamond films. Threshold fields as low as 1 to 3 V/μm have been found for samples having large amount of sp^2-bonded carbon phase. On the contrary, poor emission is obtained for the dominant diamond phase.

Importantly, it has also been demonstrated that the threshold field can be reduced when growing CVD diamond with several structural defects [140]. Correlation between the threshold field and the width of the diamond Raman peak (used to quantify the defect density) was reported and explained considering that the various types of defects in the diamond structure can create additional energy bands within the diamond band gap, contributing to FE at low fields.

Doped diamonds have been also widely investigated [134,141]. By comparing B-, Li-, P-, and N-doped diamonds and different treatments it has been demonstrated that one of the lowest reported field ~0.2 V/μm, can be obtained for N-doped diamond samples after a complex surface

treatment with O_2 plasma, coated with Cs, heated, and exposed to O_2. The FE improvement has been explained by taking into account that the diamond surface is oxygen terminated, due to the action of O_2 plasma, and consequently reacts with Cs to form an oxygen-stable diamond–O–Cs surface, which lowers the work function of diamond.

It has been recognized that diamond-based electron emitters with negative electron affinity are suitable for the realization of vacuum power switches [142]. High current density and uniformity represent the most relevant feature of the switch, and many conventional field emitters are not suitable for such a purpose. On the contrary, hydrogen-terminated diamond is the best material to be exploited due to its negative electron affinity [143–146]. Experiments of total photoelectron yield spectroscopy [142] have clearly demonstrated that PN and PIN junctions are an effective method of using negative electron affinity for emitting devices [143,147]. Moreover, Kono and Koizumi have demonstrated that electron emission from {111} PN junction diodes can be realized, obtaining negative electron affinity through surface hydrogen-termination [148]. They also achieved high electron emission efficiency (close to 10%) and 1 µA emission current. Takeuchi et al. [142] fabricated a diamond {111} P-I-N diode with an N^+ top layer and thick high-quality (insulating) I-layer. Field emission experiments were performed using a W-needle as an anode (curvature radius of 25 µm) placed 100 µm above the diode. Field emission was not observed before the hydrogenation process; such a result demonstrated that electron emission was a result of the negative electron affinity of the diamond surface. Accordingly, a 10 kV vacuum power switch using diamond P-I-N electron emitter has been developed and characterized [142] as showing a breakthrough power transmission efficiency of 73% at 9.8 kV during operation at room temperature. Such a result was explained as a combination of the negative electron affinity of the diamond surface, and a high level of electron injection with a hopping conduction-type in the N^+ layer. Importantly, these findings open a path for the development of vacuum power switches operating at 100 kV with an efficiency beyond 99.9%.

2.7. Emission from Graphene and Graphitic Materials

The most stable allotrope of carbon is three-dimensional graphite, known since 1789, although until 2004 it was impossible to isolate a single graphite layer. Then, Novoselov and Geim [149] succeeded in producing a monolayer graphene by mechanical exfoliation from highly ordered pyrolytic graphite. Graphene is the natural building block of any graphitic material. Since its discovery it has been exploited for back-gated field effect transistors [149–152], hybrid photodiode [153,154], and several other nano-electronics applications [155,156].

Several studies on graphene films demonstrated that the FE from graphene edges or pleats occurs at low applied fields [157–159]. A graphene layer exfoliated or directly grown on a substrate is not the most suitable for FE, because the planar geometry suppresses field enhancement [160]. Despite this, Santandrea et al. [38] demonstrated that emitted current up to 1 µA can occur from the flat part of graphene flakes, likely favored by graphene wrinkles, under applied fields of ∼600 V/µm and with significant stability over a period of several hours.

Field emission from graphene is challenging because the deposition methods typically lead to sheets that lay flat on the substrate surface, which limits the field enhancement.

Wet transferred suspended graphene fabricated on interdigitated electrodes [161] has been demonstrated as a high-quality emitter. It has been shown that the suspended graphene has better emission properties (from the whole surface) compared to the graphene commonly exfoliated on flat substrates. However, fields as high as 170 V/µm are necessary to extract electrons from the graphene layer and to fully exploit the FE capabilities of graphene it is convenient to arrange graphene flakes perpendicular to the substrate to favor the emission from the sharp edges. It has been reported [162] that dispersion of graphene in polystyrene and successive deposition of composite allow graphene sheets to be somewhat aligned. In particular, it has been demonstrated that the orientation of graphene sheets can be modified from randomly oriented to laterally oriented by tuning the spin coating speed. This method realizes graphene/polymer composite thin films with oriented graphene sheets at certain

angles on a Si substrate. Such orientation causes an important field enhancement factor up to 1.2×10^3 allowing FE at turn-on field as low as 4 V/µm. By applying the same method on Si microtips, it has been demonstrated that FE can be turned on at lower fields, ~2.3 V/µm [163].

A different technique, based on microwave plasma enhanced CVD, has been also applied to realize vertically aligned graphene sheets on Ti or Si substrates [164]. Remarkably, a lower turn-on field of about 1 V/µm was obtained for few layers of graphene grown on titanium. The main drawback of this method remains the difficulty of controlling graphene sheet density with related problems arising due to the screening effect in high density systems.

Exfoliated graphene has also been investigated for FE applications by using either screen printing techniques [158], or electrophoretic deposition [165] reporting turn-on field up to 5.2 V/µm. A comparative study on the FE performance of graphene oxide (initially exfoliated by modified Hummers method), reduced either by hydrazine or by microwave assistance, has been reported [166] with the result of improved turn-on field in case of microwave-reduced graphene ($E_{on} = 0.39$ V/µm vs. $E_{on} = 0.94$ V/µm). This experimental observation has been explained by the presence of larger graphene sheets, and the microwave reduction not breaking the large sheets into small pieces during the process, contrary to what happens with hydrazine reduction. Consequently, larger sheets favor natural rolls and tips because of the higher surface tension, with clear benefit to FE performances. Pandey et al. [167] demonstrated an improved FE (higher current density and lower turn-on field) with respect to planar graphene when introducing morphological disorder (such as edges, discontinuity and ripples) in thermal-CVD graphene due to the poor adhesion on Si (100) substrates.

A different approach, concerning growth of graphene on CNT or nanostructures, has been also intensively investigated. Deng et al. [168,169] reported excellent FE from few-layer graphene (FLG)–carbon nanotube hybrids synthesized using radio frequency hydrogen plasma sputtering deposition. They obtained few-layer graphene sheets sparsely distributed on top of CNTs with about 2–10 layer sharp edges (see Figure 6). Such a unique structure offers advantages from both the high aspect ratio of CNTs as well as from the sharp edges of flakes, resulting in a turn-on field below 1 V/µm and a field enhancement factor of about 4000.
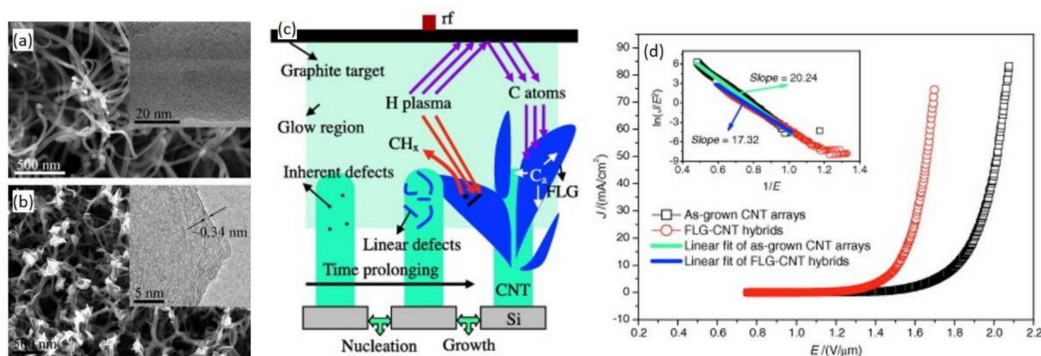
Figure 6. (**a**,**b**) SEM image of few-layer graphene–CNT hybrids (the inset is a TEM image showing a hybrid structure between a CNT and a FLG); (**c**) Schematic of a two-step few-layer graphene growth model: nucleation and 2D growth; (**d**) FE properties of the as-grown CNT arrays and the FLG–CNT hybrids (the corresponding F–N plots in the inset is). Image adapted with permission from [168], Copyright Elsevier, 2012.

Several studies have examined the transfer of graphene on different structures in order to realize high performance emitting cathodes. Deposition of graphene oxide (exfoliated from graphite and made into solution drops) on Ni nano-tips has been reported [170], demonstrating that the sheets supported on nanometer-scale sharp Ni nano-tip arrays behave as excellent field emitters, not depending on the alignment of the sheets with the electric field, with a turn-on field as low as 0.5 V/µm. Iemmo et al. [30]

also demonstrated that the FE characteristics of InP nanocrystals were enhanced by placing a graphene monolayer on the nanocrystal array.

It has been reported that graphene can be used to realize hybrid structured Si-nanowires/graphene for FE purposes [171]. Such configuration allows the creation of uniform protrusions in graphene, starting from well-aligned silicon nanowires of different diameters (from 400 to 600 nm). It has been demonstrated that large-scale CVD-graphene transferred onto the ordered array, significantly improve the FE performance with respect to nanowires alone, due to the formation of regular undulations of the graphene layer. The reported values of the turn-on field were in the range 2.0 to 2.6 V/μm depending on the nanowire diameter, while the estimated enhancement factor was from 4000 to 6500. The hybrid structure realized with nanowires having a 600 nm diameter, exhibit the lowest turn-on field and highest β values, because it realizes more contact points and protrusions, favoring electron transfer. Indeed, the protrusions are a crucial element responsible for the field emission properties of the hybrid structure.

Graphene samples produced by the arc-discharge method in a hydrogen atmosphere have been characterized as field emitters either as undoped and as nitrogen- and boron-doped samples [172]. Graphene sheets have been vertically oriented in order by means of electrophoretic deposition on Si substrate to enhance the FE properties. To achieve a current density of 10 μA/cm^2 a turn-on field of 0.7, 0.8, and 0.6 V/μm for undoped, boron-doped, and nitrogen-doped graphene, respectively, have been reported. Such values are remarkably lower than the values reported for graphene samples [158,165,173] and sub-nanometer graphite sheets [174]. The FE behavior is explained in terms of the nanometric features of graphene and the resonance tunneling phenomenon. Finally, the lowest turn-on field for N-doped graphene was identified as the result of the up-shift of the Fermi level of graphene due to N-doping [175].

By using photolithography and wet etching processes, well-aligned graphene field emission arrays (FEA) have been fabricated on copper foil [176]. This method realizes high-ordered micro sized graphene pattern arrays on copper foil with a diameter of 4 mm, forming about 6000 emitting elements (of about 30 μm × 30 μm), with 20 μm separation. FE characterization has demonstrated a turn-on field of 7.2 V/μm for a current of 100 nA/cm^2. In comparison, negligible current was recorded by applying similar fields on un-patterned graphene layers on copper. Lin et al. [177] developed a graphene-sheets/ZnO-nanorods hybrid structure on glass substrate by means of sputtering and hydrothermal techniques. CVD-graphene on copper is transferred on ZnO nanorods to realize a hybrid structure with improved FE characteristics in comparison to the ZnO nanorods alone. The lowest turn-on field reported is 3.7 V/μm at 1 μA/cm^2, and the field enhancement factor has been estimated as β = 8723. They demonstrated that the presence of graphene sheets decreases the work function in the hybrid structure, and also increases the number of additional emission sites.

3. Conclusions

Many theoretical and experimental studies over the past thirty years have focused on the synthesis and field emission mechanisms of carbon materials. Nevertheless, there are still many challenges to overcome on the way to real applications, including emission uniformity and stability, large-scale fabrication, the lifetime of the emitting source, costs, etc. Much endeavor is currently addressing the development of novel carbon-based cathodes, such as graphene on patterned nanostructures or graphene/CNTs hybrids devices.

This review has shown the great potential of carbon nanostructure to develop new field emission devices and the status of the research in the field.

Conflicts of Interest: The authors declare no conflict of interest.

References

1. Saito, Y.; Hata, K.; Takakura, A.; Yotani, J.; Uemura, S. Field emission of carbon nanotubes and its application as electron sources of ultra-high luminance light-source devices. *Phys. B Condens. Matter* **2002**, *323*, 30–37. [CrossRef]

2. Talin, A.A.; Dean, K.A.; Jaskie, J.E. Field emission displays: A critical review. *Solid-State Electron.* **2001**, *45*, 963–976. [CrossRef]

3. Wang, Q.H.; Yan, M.; Chang, R.P.H. Flat panel display prototype using gated carbon nanotube field emitters. *Appl. Phys. Lett.* **2001**, *78*, 1294–1296. [CrossRef]

4. Swanson, L.W.; Schwind, G.A. A Review of Field Electron Source Use in Electron Microscopes. *Microsc. Microanal.* **2005**, *11*. [CrossRef]

5. Fursey, G.N. *Field Emission in Vacuum Microelectronics*; Microdevices; Kluwer Academic/Plenum Publishers: New York, NY, USA, 2005; ISBN 978-0-306-47450-7.

6. Radauscher, E.J.; Gilchrist, K.H.; Di Dona, S.T.; Russell, Z.E.; Piascik, J.R.; Amsden, J.J.; Parker, C.B.; Stoner, B.R.; Glass, J.T. The improved perfomance of field emission vacuum microelectronic devices for integrated circuits. *IEEE Trans. Electron Dev.* **2016**, *63*, 3753–3760. [CrossRef]

7. Murphy, E.L.; Good, R.H. Thermionic Emission, Field Emission, and the Transition Region. *Phys. Rev.* **1956**, *102*, 1464–1473. [CrossRef]

8. Yamamoto, S. Fundamental physics of vacuum electron sources. *Rep. Prog. Phys.* **2006**, *69*, 181–232. [CrossRef]

9. Gomer, R. *Field Emission and Field Ionization*; Harvard University Press: Cambridge, MA, USA, 1961.

10. Fowler, R.H.; Nordheim, L. Electron Emission in Intense Electric Fields. *Proc. R. Soc. A Math. Phys. Eng. Sci.* **1928**, *119*, 173–181. [CrossRef]

11. Froman, N. *JWKB Approximation: Contributions to the Theory*; Elsevier Science Publishing Co Inc.: Amsterdam, The Netherlands, 1965.

12. Di Bartolomeo, A.; Scarfato, A.; Giubileo, F.; Bobba, F.; Biasiucci, M.; Cucolo, A.M.; Santucci, S.; Passacantando, M. A local field emission study of partially aligned carbon-nanotubes by atomic force microscope probe. *Carbon* **2007**, *45*, 2957–2971. [CrossRef]

13. Passacantando, M.; Bussolotti, F.; Santucci, S.; Di Bartolomeo, A.; Giubileo, F.; Iemmo, L.; Cucolo, A.M. Field emission from a selected multiwall carbon nanotube. *Nanotechnology* **2008**, *19*, 395701. [CrossRef] [PubMed]

14. Edgcombe, C.J. Development of Fowler-Nordheim theory for a spherical field emitter. *Phys. Rev. B* **2005**, *72*. [CrossRef]

15. Edgcombe, C.J.; Johansen, A.M. Current–voltage characteristics of nonplanar cold field emitters. *J. Vac. Sci. Technol. B Microelectron. Nanometer Struct.* **2003**, *21*, 1519. [CrossRef]

16. Forbes, R.G. Call for experimental test of a revised mathematical form for empirical field emission current-voltage characteristics. *Appl. Phys. Lett.* **2008**, *92*, 193105. [CrossRef]

17. Forbes, R.G.; Deane, J.H.B. Reformulation of the standard theory of Fowler–Nordheim tunnelling and cold field electron emission. *Proc. R. Soc. A Math. Phys. Eng. Sci.* **2007**, *463*, 2907–2927. [CrossRef]

18. Forbes, R.G. Extraction of emission parameters for large-area field emitters, using a technically complete Fowler–Nordheim-type equation. *Nanotechnology* **2012**, *23*, 095706. [CrossRef] [PubMed]

19. Jensen, K.L. Exchange-correlation, dipole, and image charge potentials for electron sources: Temperature and field variation of the barrier height. *J. Appl. Phys.* **1999**, *85*, 2667–2680. [CrossRef]

20. Lang, N.D.; Yacoby, A.; Imry, Y. Theory of a single-atom point source for electrons. *Phys. Rev. Lett.* **1989**, *63*, 1499–1502. [CrossRef] [PubMed]

21. Gohda, Y.; Nakamura, Y.; Watanabe, K.; Watanabe, S. Self-Consistent Density Functional Calculation of Field Emission Currents from Metals. *Phys. Rev. Lett.* **2000**, *85*, 1750–1753. [CrossRef] [PubMed]

22. Maiti, A.; Andzelm, J.; Tanpipat, N.; von Allmen, P. Effect of Adsorbates on Field Emission from Carbon Nanotubes. *Phys. Rev. Lett.* **2001**, *87*. [CrossRef]

23. Han, S.; Lee, M.H.; Ihm, J. Dynamical simulation of field emission in nanostructures. *Phys. Rev. B* **2002**, *65*. [CrossRef]

24. Tada, K.; Watanabe, K. *Ab Initio* Study of Field Emission from Graphitic Ribbons. *Phys. Rev. Lett.* **2002**, *88*. [CrossRef] [PubMed]

25. Choi, Y.; Michan, M.; Johnson, J.L.; Naieni, A.K.; Ural, A.; Nojeh, A. Field-emission properties of individual GaN nanowires grown by chemical vapor deposition. *J. Appl. Phys.* **2012**, *111*, 044308. [CrossRef]

26. Lee, C.J.; Lee, T.J.; Lyu, S.C.; Zhang, Y.; Ruh, H.; Lee, H.J. Field emission from well-aligned zinc oxide nanowires grown at low temperature. *Appl. Phys. Lett.* **2002**, *81*, 3648–3650. [CrossRef]

27. Giubileo, F.; Di Bartolomeo, A.; Iemmo, L.; Luongo, G.; Passacantando, M.; Koivusalo, E.; Hakkarainen, T.; Guina, M. Field Emission from Self-Catalyzed GaAs Nanowires. *Nanomaterials* **2017**, *7*, 275. [CrossRef] [PubMed]

28. Wang, B.; Zheng, Z.; Wu, H.; Zhu, L. Field emission properties and growth mechanism of In2O3 nanostructures. *Nanoscale Res. Lett.* **2014**, *9*, 111. [CrossRef] [PubMed]

29. Di Bartolomeo, A.; Passacantando, M.; Niu, G.; Schlykow, V.; Lupina, G.; Giubileo, F.; Schroeder, T. Observation of field emission from GeSn nanoparticles epitaxially grown on silicon nanopillar arrays. *Nanotechnology* **2016**, *27*, 485707. [CrossRef] [PubMed]

30. Iemmo, L.; Di Bartolomeo, A.; Giubileo, F.; Luongo, G.; Passacantando, M.; Niu, G.; Hatami, F.; Skibitzki, O.; Schroeder, T. Graphene enhanced field emission from InP nanocrystals. *Nanotechnology* **2017**, *28*, 495705. [CrossRef] [PubMed]

31. Lin, P.-H.; Sie, C.-L.; Chen, C.-A.; Chang, H.-C.; Shih, Y.-T.; Chang, H.-Y.; Su, W.-J.; Lee, K.-Y. Field Emission Characteristics of the Structure of Vertically Aligned Carbon Nanotube Bundles. *Nanoscale Res. Lett.* **2015**, *10*. [CrossRef] [PubMed]

32. Giubileo, F.; Di Bartolomeo, A.; Scarfato, A.; Iemmo, L.; Bobba, F.; Passacantando, M.; Santucci, S.; Cucolo, A.M. Local probing of the field emission stability of vertically aligned multi-walled carbon nanotubes. *Carbon* **2009**, *47*, 1074–1080. [CrossRef]

33. Wang, M.S.; Peng, L.-M.; Wang, J.Y.; Chen, Q. Electron Field Emission Characteristics and Field Evaporation of a Single Carbon Nanotube. *J. Phys. Chem. B* **2005**, *109*, 110–113. [CrossRef] [PubMed]

34. Di, Y.; Xiao, M.; Zhang, X.; Wang, Q.; Li, C.; Lei, W.; Cui, Y. Large and stable emission current from synthesized carbon nanotube/fiber network. *J. Appl. Phys.* **2014**, *115*, 064305. [CrossRef]

35. Giubileo, F.; Di Bartolomeo, A.; Sarno, M.; Altavilla, C.; Santandrea, S.; Ciambelli, P.; Cucolo, A.M. Field emission properties of as-grown multiwalled carbon nanotube films. *Carbon* **2012**, *50*, 163–169. [CrossRef]

36. Giubileo, F.; Iemmo, L.; Luongo, G.; Martucciello, N.; Raimondo, M.; Guadagno, L.; Passacantando, M.; Lafdi, K.; Di Bartolomeo, A. Transport and field emission properties of buckypapers obtained from aligned carbon nanotubes. *J. Mater. Sci.* **2017**, *52*, 6459–6468. [CrossRef]

37. Kumar, S.; Duesberg, G.S.; Pratap, R.; Raghavan, S. Graphene field emission devices. *Appl. Phys. Lett.* **2014**, *105*, 103107. [CrossRef]

38. Santandrea, S.; Giubileo, F.; Grossi, V.; Santucci, S.; Passacantando, M.; Schroeder, T.; Lupina, G.; Di Bartolomeo, A. Field emission from single and few-layer graphene flakes. *Appl. Phys. Lett.* **2011**, *98*, 163109. [CrossRef]

39. Di Bartolomeo, A.; Giubileo, F.; Iemmo, L.; Romeo, F.; Russo, S.; Unal, S.; Passacantando, M.; Grossi, V.; Cucolo, A.M. Leakage and field emission in side-gate graphene field effect transistors. *Appl. Phys. Lett.* **2016**, *109*, 023510. [CrossRef]

40. Urban, F.; Passacantando, M.; Giubileo, F.; Iemmo, L.; Di Bartolomeo, A. Transport and Field Emission Properties of MoS2 Bilayers. *Nanomaterials* **2018**, *8*, 151. [CrossRef] [PubMed]

41. Suryawanshi, S.R.; Pawbake, A.S.; Pawar, M.S.; Jadkar, S.R.; More, M.A.; Late, D.J. Enhanced field emission behavior of layered MoSe2. *Mater. Res. Express* **2016**, *3*, 035003. [CrossRef]

42. Yuasa, K.; Shimoi, A.; Ohba, I.; Oshima, C. Modified Fowler–Nordheim field emission formulae from a nonplanar emitter model. *Surf. Sci.* **2002**, *520*, 18–28. [CrossRef]

43. Spindt, C.A. A Thin-Film Field-Emission Cathode. *J. Appl. Phys.* **1968**, *39*, 3504–3505. [CrossRef]

44. Ghis, A.; Meyer, R.; Rambaud, P.; Levy, F.; Leroux, T. Sealed vacuum devices: Fluorescent microtip displays. *IEEE Trans. Electron Devices* **1991**, *38*, 2320–2322. [CrossRef]

45. Fan, Y.; Rose, M. Field Emission Displays (FEDs). In *Handbook of Visual Display Technology*; Chen, J., Cranton, W., Fihn, M., Eds.; Springer: Berlin/Heidelberg, Germany, 2012; pp. 1071–1104. ISBN 978-3-540-79566-7.

46. Iijima, S. Helical microtubules of graphitic carbon. *Nature* **1991**, *354*, 56–58. [CrossRef]

47. Bethune, D.S.; Kiang, C.H.; de Vries, M.S.; Gorman, G.; Savoy, R.; Vazquez, J.; Beyers, R. Cobalt-catalysed growth of carbon nanotubes with single-atomic-layer walls. *Nature* **1993**, *363*, 605–607. [CrossRef]

48.   Iijima, S.; Ichihashi, T. Single-shell carbon nanotubes of 1-nm diameter. *Nature* **1993**, *363*, 603–605. [CrossRef]

49.   Wind, S.J.; Appenzeller, J.; Martel, R.; Derycke, V.; Avouris, P. Vertical scaling of carbon nanotube field-effect transistors using top gate electrodes. *Appl. Phys. Lett.* **2002**, *80*, 3817–3819. [CrossRef]

50.   Franklin, A.D.; Luisier, M.; Han, S.-J.; Tulevski, G.; Breslin, C.M.; Gignac, L.; Lundstrom, M.S.; Haensch, W. Sub-10 nm Carbon Nanotube Transistor. *Nano Lett.* **2012**, *12*, 758–762. [CrossRef] [PubMed]

51.   Di Bartolomeo, A.; Rinzan, M.; Boyd, A.K.; Yang, Y.; Guadagno, L.; Giubileo, F.; Barbara, P. Electrical properties and memory effects of field-effect transistors from networks of single- and double-walled carbon nanotubes. *Nanotechnology* **2010**, *21*, 115204. [CrossRef] [PubMed]

52.   Di Bartolomeo, A.; Yang, Y.; Rinzan, M.B.M.; Boyd, A.K.; Barbara, P. Record Endurance for Single-Walled Carbon Nanotube–Based Memory Cell. *Nanoscale Res. Lett.* **2010**, *5*, 1852–1855. [CrossRef] [PubMed]

53.   Dai, H.; Hafner, J.H.; Rinzler, A.G.; Colbert, D.T.; Smalley, R.E. Nanotubes as nanoprobes in scanning probe microscopy. *Nature* **1996**, *384*, 147–150. [CrossRef]

54.   Zhou, P.; Yang, X.; He, L.; Hao, Z.; Luo, W.; Xiong, B.; Xu, X.; Niu, C.; Yan, M.; Mai, L. The Young's modulus of high-aspect-ratio carbon/carbon nanotube composite microcantilevers by experimental and modeling validation. *Appl. Phys. Lett.* **2015**, *106*, 111908. [CrossRef]

55.   Gao, X.P.; Lan, Y.; Pan, G.L.; Wu, F.; Qu, J.Q.; Song, D.Y.; Shen, P.W. Electrochemical Hydrogen Storage by Carbon Nanotubes Decorated with Metallic Nickel. *Electrochem. Solid-State Lett.* **2001**, *4*, A173. [CrossRef]

56.   Kaempgen, M.; Chan, C.K.; Ma, J.; Cui, Y.; Gruner, G. Printable Thin Film Supercapacitors Using Single-Walled Carbon Nanotubes. *Nano Lett.* **2009**, *9*, 1872–1876. [CrossRef] [PubMed]

57.   Dai, L.; Chang, D.W.; Baek, J.-B.; Lu, W. Carbon Nanomaterials for Advanced Energy Conversion and Storage. *Small* **2012**, *8*, 1130–1166. [CrossRef] [PubMed]

58.   King, P.J.; Higgins, T.M.; De, S.; Nicoloso, N.; Coleman, J.N. Percolation Effects in Supercapacitors with Thin, Transparent Carbon Nanotube Electrodes. *ACS Nano* **2012**, *6*, 1732–1741. [CrossRef] [PubMed]

59.   Wu, Z. Transparent, Conductive Carbon Nanotube Films. *Science* **2004**, *305*, 1273–1276. [CrossRef] [PubMed]

60.   Zhang, D.; Ryu, K.; Liu, X.; Polikarpov, E.; Ly, J.; Tompson, M.E.; Zhou, C. Transparent, Conductive, and Flexible Carbon Nanotube Films and Their Application in Organic Light-Emitting Diodes. *Nano Lett.* **2006**, *6*, 1880–1886. [CrossRef] [PubMed]

61.   Zhao, Y.; Wei, J.; Vajtai, R.; Ajayan, P.M.; Barrera, E.V. Iodine doped carbon nanotube cables exceeding specific electrical conductivity of metals. *Sci. Rep.* **2011**, *1*. [CrossRef] [PubMed]

62.   Rinzler, A.G.; Hafner, J.H.; Nikolaev, P.; Nordlander, P.; Colbert, D.T.; Smalley, R.E.; Lou, L.; Kim, S.G.; Tomanek, D. Unraveling Nanotubes: Field Emission from an Atomic Wire. *Science* **1995**, *269*, 1550–1553. [CrossRef] [PubMed]

63.   De Heer, W.A.; Châtelain, A.; Ugarte, D. A Carbon Nanotube Field-Emission Electron Source. *Science* **1995**, *270*, 1179–1180. [CrossRef]

64.   Wang, X.; Li, Q.; Xie, J.; Jin, Z.; Wang, J.; Li, Y.; Jiang, K.; Fan, S. Fabrication of Ultralong and Electrically Uniform Single-Walled Carbon Nanotubes on Clean Substrates. *Nano Lett.* **2009**, *9*, 3137–3141. [CrossRef] [PubMed]

65.   Lan, Y.; Wang, Y.; Ren, Z.F. Physics and applications of aligned carbon nanotubes. *Adv. Phys.* **2011**, *60*, 553–678. [CrossRef]

66.   Nishikawa, O.; Tomitori, M.; Iwawaki, F. High resolution tunneling microscopies: From FEM to STS. *Surf. Sci.* **1992**, *266*, 204–213. [CrossRef]

67.   Xu, N.S.; Huq, S.E. Novel cold cathode materials and applications. *Mater. Sci. Eng. R Rep.* **2005**, *48*, 47–189. [CrossRef]

68.   Sugie, H.; Tanemura, M.; Filip, V.; Iwata, K.; Takahashi, K.; Okuyama, F. Carbon nanotubes as electron source in an X-ray tube. *Appl. Phys. Lett.* **2001**, *78*, 2578–2580. [CrossRef]

69.   Yue, G.Z.; Qiu, Q.; Gao, B.; Cheng, Y.; Zhang, J.; Shimoda, H.; Chang, S.; Lu, J.P.; Zhou, O. Generation of continuous and pulsed diagnostic imaging X-ray radiation using a carbon-nanotube-based field-emission cathode. *Appl. Phys. Lett.* **2002**, *81*, 355–357. [CrossRef]

70.   Choi, W.B.; Chung, D.S.; Kang, J.H.; Kim, H.Y.; Jin, Y.W.; Han, I.T.; Lee, Y.H.; Jung, J.E.; Lee, N.S.; Park, G.S.; et al. Fully sealed, high-brightness carbon-nanotube field-emission display. *Appl. Phys. Lett.* **1999**, *75*, 3129–3131. [CrossRef]

71.   Baughman, R.H. Carbon Nanotubes—The Route toward Applications. *Science* **2002**, *297*, 787–792. [CrossRef] [PubMed]

72. Dresselhaus, M.S.; Dresselhaus, G.; Avouris, P. (Eds.) Carbon Nanotubes Synthesis, Structure, Properties, and Applications. In *Topics in Applied Physics*; Springer: Berlin/Heidelberg, Germany, 2001; Volume 80, ISBN 978-3-540-41086-7.

73. Charlier, J.-C.; Blase, X.; Roche, S. Electronic and transport properties of nanotubes. *Rev. Mod. Phys.* **2007**, *79*, 677–732. [CrossRef]

74. Edgcombe, C.J.; Valdre, U. Microscopy and computational modelling to elucidate the enhancement factor for field electron emitters. *J. Microsc.* **2001**, *203*, 188–194. [CrossRef]

75. Bonard, J.-M.; Maier, F.; Stöckli, T.; Châtelain, A.; de Heer, W.A.; Salvetat, J.-P.; Forró, L. Field emission properties of multiwalled carbon nanotubes. *Ultramicroscopy* **1998**, *73*, 7–15. [CrossRef]

76. Smith, R.C.; Silva, S.R.P. Interpretation of the field enhancement factor for electron emission from carbon nanotubes. *J. Appl. Phys.* **2009**, *106*, 014314. [CrossRef]

77. Wang, M.; Li, Z.H.; Shang, X.F.; Wang, X.Q.; Xu, Y.B. Field-enhancement factor for carbon nanotube array. *J. Appl. Phys.* **2005**, *98*, 014315. [CrossRef]

78. Wang, X.Q.; Wang, M.; He, P.M.; Xu, Y.B.; Li, Z.H. Model calculation for the field enhancement factor of carbon nanotube. *J. Appl. Phys.* **2004**, *96*, 6752–6755. [CrossRef]

79. DeHeer, W.A.; Bacsa, W.S.; Chatelain, A.; Gerfin, T.; Humphrey-Baker, R.; Forro, L.; Ugarte, D. Aligned Carbon Nanotube Films: Production and Optical and Electronic Properties. *Science* **1995**, *268*, 845–847. [CrossRef] [PubMed]

80. Bower, C.; Zhou, O.; Zhu, W.; Ramirez, A.G.; Kochanski, G.P.; Jin, S. Fabrication and Field Emission Properties of Carbon Nanotube Cathodes. *MRS Proc.* **1999**, *593*. [CrossRef]

81. Collins, P.G.; Zettl, A. A simple and robust electron beam source from carbon nanotubes. *Appl. Phys. Lett.* **1996**, *69*, 1969–1971. [CrossRef]

82. Wang, L.; Chen, Y.; Chen, T.; Que, W.; Sun, Z. Optimization of field emission properties of carbon nanotubes cathodes by electrophoretic deposition. *Mater. Lett.* **2007**, *61*, 1265–1269. [CrossRef]

83. Feng, T.; Dai, L.; Jiang, J.; Wang, X.; Liu, X.; Zou, S.; Li, Q.; Xu, J. Memory emission of printed carbon nanotube cathodes. *Appl. Phys. Lett.* **2006**, *88*, 203108. [CrossRef]

84. Wang, Q.H.; Setlur, A.A.; Lauerhaas, J.M.; Dai, J.Y.; Seelig, E.W.; Chang, R.P.H. A nanotube-based field-emission flat panel display. *Appl. Phys. Lett.* **1998**, *72*, 2912–2913. [CrossRef]

85. Burghard, M.; Duesberg, G.; Philipp, G.; Muster, J.; Roth, S. Controlled Adsorption of Carbon Nanotubes on Chemically Modified Electrode Arrays. *Adv. Mater.* **1998**, *10*, 584–588. [CrossRef]

86. Bonard, J.-M.; Kind, H.; Stöckli, T.; Nilsson, L.-O. Field emission from carbon nanotubes: The first five years. *Solid-State Electron.* **2001**, *45*, 893–914. [CrossRef]

87. Bonard, J.-M.; Croci, M.; Klinke, C.; Kurt, R.; Noury, O.; Weiss, N. Carbon nanotube films as electron field emitters. *Carbon* **2002**, *40*, 1715–1728. [CrossRef]

88. Zhu, W.; Bower, C.; Zhou, O.; Kochanski, G.; Jin, S. Large current density from carbon nanotube field emitters. *Appl. Phys. Lett.* **1999**, *75*, 873–875. [CrossRef]

89. Obraztsov, A.N.; Volkov, A.P.; Pavlovskii, I.Y.; Chuvilin, A.L.; Rudina, N.A.; Kuznetsov, V.L. Role of the curvature of atomic layers in electron field emission from graphitic nanostructured carbon. *J. Exp. Theor. Phys. Lett.* **1999**, *69*, 411–417. [CrossRef]

90. Nilsson, L.; Groening, O.; Emmenegger, C.; Kuettel, O.; Schaller, E.; Schlapbach, L.; Kind, H.; Bonard, J.-M.; Kern, K. Scanning field emission from patterned carbon nanotube films. *Appl. Phys. Lett.* **2000**, *76*, 2071–2073. [CrossRef]

91. Ito, F.; Tomihari, Y.; Okada, Y.; Konuma, K.; Okamoto, A. Carbon-nanotube-based triode-field-emission displays using gated emitter structure. *IEEE Electron Device Lett.* **2001**, *22*, 426–428. [CrossRef]

92. Chung, D.-S.; Park, S.H.; Lee, H.W.; Choi, J.H.; Cha, S.N.; Kim, J.W.; Jang, J.E.; Min, K.W.; Cho, S.H.; Yoon, M.J.; et al. Carbon nanotube electron emitters with a gated structure using backside exposure processes. *Appl. Phys. Lett.* **2002**, *80*, 4045–4047. [CrossRef]

93. Thong, J.T.L.; Oon, C.H.; Eng, W.K.; Zhang, W.D.; Gan, L.M. High-current field emission from a vertically aligned carbon nanotube field emitter array. *Appl. Phys. Lett.* **2001**, *79*, 2811–2813. [CrossRef]

94. Jo, S.H.; Tu, Y.; Huang, Z.P.; Carnahan, D.L.; Huang, J.Y.; Wang, D.Z.; Ren, Z.F. Correlation of field emission and surface microstructure of vertically aligned carbon nanotubes. *Appl. Phys. Lett.* **2004**, *84*, 413–415. [CrossRef]

95.	Sveningsson, M.; Morjan, R.E.; Nerushev, O.; Campbell, E.E.B. Electron field emission from multi-walled carbon nanotubes. *Carbon* **2004**, *42*, 1165–1168. [CrossRef]

96.	Saito, Y.; Uemura, S. Field emission from carbon nanotubes and its application to electron sources. *Carbon* **2000**, *38*, 169–182. [CrossRef]

97.	Fursey, G. Field emission in vacuum micro-electronics. *Appl. Surf. Sci.* **2003**, *215*, 113–134. [CrossRef]

98.	Kwo, J.L.; Yokoyama, M.; Wang, W.C.; Chuang, F.Y.; Lin, I.N. Characteristics of flat panel display using carbon nanotubes as electron emitters. *Diam. Relat. Mater.* **2000**, *9*, 1270–1274. [CrossRef]

99.	Li, C.; Zhang, Y.; Mann, M.; Hasko, D.; Lei, W.; Wang, B.; Chu, D.; Pribat, D.; Amaratunga, G.A.J.; Milne, W.I. High emission current density, vertically aligned carbon nanotube mesh, field emitter array. *Appl. Phys. Lett.* **2010**, *97*, 113107. [CrossRef]

100.	Wadhawan, A.; Stallcup, R.E.; Stephens, K.F.; Perez, J.M.; Akwani, I.A. Effects of O_2, Ar, and H_2 gases on the field-emission properties of single-walled and multiwalled carbon nanotubes. *Appl. Phys. Lett.* **2001**, *79*, 1867–1869. [CrossRef]

101.	Purcell, S.T.; Vincent, P.; Journet, C.; Binh, V.T. Hot Nanotubes: Stable Heating of Individual Multiwall Carbon Nanotubes to 2000 K Induced by the Field-Emission Current. *Phys. Rev. Lett.* **2002**, *88*. [CrossRef] [PubMed]

102.	Bonard, J.-M.; Klinke, C.; Dean, K.A.; Coll, B.F. Degradation and failure of carbon nanotube field emitters. *Phys. Rev. B* **2003**, *67*. [CrossRef]

103.	Dean, K.A.; Chalamala, B.R. The environmental stability of field emission from single-walled carbon nanotubes. *Appl. Phys. Lett.* **1999**, *75*, 3017–3019. [CrossRef]

104.	Suga, H.; Abe, H.; Tanaka, M.; Shimizu, T.; Ohno, T.; Nishioka, Y.; Tokumoto, H. Stable multiwalled carbon nanotube electron emitter operating in low vacuum. *Surf. Interface Anal.* **2006**, *38*, 1763–1767. [CrossRef]

105.	Kita, S.; Sakai, Y.; Endo, T.; Sugimoto, W.; Goto, H. Stabilization of field electron emission from carbon nanofibers using ballast resistance. *J. Vac. Sci. Technol. Nanotechnol. Microelectron. Mater. Process. Meas. Phenom.* **2012**, *30*, 031801. [CrossRef]

106.	Shimoi, N.; Estrada, A.L.; Tanaka, Y.; Tohji, K. Properties of a field emission lighting plane employing highly crystalline single-walled carbon nanotubes fabricated by simple processes. *Carbon* **2013**, *65*, 228–235. [CrossRef]

107.	Shimoi, N.; Tohji, K. Current-Fluctuation Mechanism of Field Emitters Using Metallic Single-Walled Carbon Nanotubes with High Crystallinity. *Appl. Sci.* **2017**, *7*, 1322. [CrossRef]

108.	Smith, R.C.; Cox, D.C.; Silva, S.R.P. Electron field emission from a single carbon nanotube: Effects of anode location. *Appl. Phys. Lett.* **2005**, *87*, 103112. [CrossRef]

109.	Xu, Z.; Bai, X.D.; Wang, E.G.; Wang, Z.L. Field emission of individual carbon nanotube with *in situ* tip image and real work function. *Appl. Phys. Lett.* **2005**, *87*, 163106. [CrossRef]

110.	Nojeh, A.; Wong, W.-K.; Yieh, E.; Pease, R.F.; Dai, H. Electron beam stimulated field-emission from single-walled carbon nanotubes. *J. Vac. Sci. Technol. B Microelectron. Nanometer Struct.* **2004**, *22*, 3124. [CrossRef]

111.	Bonard, J.-M.; Salvetat, J.-P.; Stöckli, T.; de Heer, W.A.; Forró, L.; Châtelain, A. Field emission from single-wall carbon nanotube films. *Appl. Phys. Lett.* **1998**, *73*, 918–920. [CrossRef]

112.	Kuzumaki, T.; Takamura, Y.; Ichinose, H.; Horiike, Y. Structural change at the carbon-nanotube tip by field emission. *Appl. Phys. Lett.* **2001**, *78*, 3699–3701. [CrossRef]

113.	Robertson, J. Realistic applications of CNTs. *Mater. Today* **2004**, *7*, 46–52. [CrossRef]

114.	Smith, R.C.; Carey, J.D.; Forrest, R.D.; Silva, S.R.P. Effect of aspect ratio and anode location on the field emission properties of a single tip based emitter. *J. Vac. Sci. Technol. B Microelectron. Nanometer Struct.* **2005**, *23*, 632. [CrossRef]

115.	Bonard, J.-M.; Dean, K.A.; Coll, B.F.; Klinke, C. Field Emission of Individual Carbon Nanotubes in the Scanning Electron Microscope. *Phys. Rev. Lett.* **2002**, *89*. [CrossRef] [PubMed]

116.	Milne, W.I.; Teo, K.B.K.; Chhowalla, M.; Amaratunga, G.A.J.; Lee, S.B.; Hasko, D.G.; Ahmed, H.; Groening, O.; Legagneux, P.; Gangloff, L.; et al. Electrical and field emission investigation of individual carbon nanotubes from plasma enhanced chemical vapour deposition. *Diam. Relat. Mater.* **2003**, *12*, 422–428. [CrossRef]

117.	Minh, P.N.; Tuyen, L.T.T.; Ono, T.; Miyashita, H.; Suzuki, Y.; Mimura, H.; Esashi, M. Selective growth of carbon nanotubes on Si microfabricated tips and application for electron field emitters. *J. Vac. Sci. Technol. B Microelectron. Nanometer Struct.* **2003**, *21*, 1705. [CrossRef]

118. She, J.C.; Xu, N.S.; Deng, S.Z.; Chen, J.; Bishop, H.; Huq, S.E.; Wang, L.; Zhong, D.Y.; Wang, E.G. Vacuum breakdown of carbon-nanotube field emitters on a silicon tip. *Appl. Phys. Lett.* **2003**, *83*, 2671–2673. [CrossRef]

119. Jin, C.; Wang, J.; Wang, M.; Su, J.; Peng, L.-M. In-situ studies of electron field emission of single carbon nanotubes inside the TEM. *Carbon* **2005**, *43*, 1026–1031. [CrossRef]

120. Hii, K.-F.; Ryan Vallance, R.; Chikkamaranahalli, S.B.; Pinar Mengüç, M.; Rao, A.M. Characterizing field emission from individual carbon nanotubes at small distances. *J. Vac. Sci. Technol. B Microelectron. Nanometer Struct.* **2006**, *24*, 1081. [CrossRef]

121. Wang, C.; Garcia, A.; Ingram, D.C.; Lake, M.; Kordesch, M.E. Cold field emission from CVD diamond films observed in emission electron microscopy. *Electron. Lett.* **1991**, *27*, 1459. [CrossRef]

122. Xu, N.S.; Tzeng, Y.; Latham, R.V. A diagnostic study of the field emission characteristics of individual micro-emitters in CVD diamond films. *J. Phys. D Appl. Phys.* **1994**, *27*, 1988–1991. [CrossRef]

123. Geis, M.W.; Gregory, J.A.; Pate, B.B. Capacitance-voltage measurements on metal-SiO/sub 2/-diamond structures fabricated with. *IEEE Trans. Electron Devices* **1991**, *38*, 619–626. [CrossRef]

124. Lettington, A.H.; Steeds, J.W. (Eds.) *Thin Film Diamond*, 1st ed.; Chapman & Hall for the Royal Society: London, UK; New York, NY, USA, 1994; ISBN 978-0-412-49630-1.

125. Xu, N. Field emission from diamond and related films. *Ultramicroscopy* **1999**, *79*, 59–72. [CrossRef]

126. Staryga, E.; Jarzynska, D.; Fabisiak, K.; Banaszak, A. Field emission from diamond and diamond-like carbon films. *J. Superhard Mater.* **2007**, *29*, 189–197. [CrossRef]

127. Robertson, J. Electron affinity of carbon systems. *Diam. Relat. Mater.* **1996**, *5*, 797–801. [CrossRef]

128. Jou, S.; Doerr, H.J.; Bunshah, R.F. Electron emission characterization of diamond thin films grown from a solid carbon source. *Thin Solid Films* **1996**, *280*, 256–261. [CrossRef]

129. Karabutov, A.; Frolov, V.; Pimenov, S.; Konov, V. Grain boundary field electron emission from CVD diamond films. *Diam. Relat. Mater.* **1999**, *8*, 763–767. [CrossRef]

130. Zhirnov, V.V. Field emission from silicon spikes with diamond coatings. *J. Vac. Sci. Technol. B Microelectron. Nanometer Struct.* **1995**, *13*, 418. [CrossRef]

131. Cui, J.B.; Ristein, J.; Ley, L. Electron Affinity of the Bare and Hydrogen Covered Single Crystal Diamond (111) Surface. *Phys. Rev. Lett.* **1998**, *81*, 429–432. [CrossRef]

132. Xu, N.S.; Latham, R.V. Coherently scattered hot electrons emitted from MIM graphite microstructures deposited on broad-area vacuum-insulated high-voltage electrodes. *J. Phys. D Appl. Phys.* **1986**, *19*, 477–482. [CrossRef]

133. Gröning, O.; Küttel, O.M.; Gröning, P.; Schlapbach, L. Field emission spectroscopy from discharge activated chemical vapor deposition diamond. *J. Vac. Sci. Technol. B Microelectron. Nanometer Struct.* **1999**, *17*, 1064. [CrossRef]

134. Geis, M.W.; Twichell, J.C.; Efremow, N.N.; Krohn, K.; Lyszczarz, T.M. Comparison of electric field emission from nitrogen-doped, type Ib diamond, and boron-doped diamond. *Appl. Phys. Lett.* **1996**, *68*, 2294–2296. [CrossRef]

135. Geis, M.W. Diamond emitters fabrication and theory. *J. Vac. Sci. Technol. B Microelectron. Nanometer Struct.* **1996**, *14*, 2060. [CrossRef]

136. Zhu, W. Electron field emission from chemical vapor deposited diamond. *J. Vac. Sci. Technol. B Microelectron. Nanometer Struct.* **1996**, *14*, 2011. [CrossRef]

137. Lacher, F.; Wild, C.; Behr, D.; Koidl, P. Electron field emission from thin fine-grained CVD diamond films. *Diam. Relat. Mater.* **1997**, *6*, 1111–1116. [CrossRef]

138. Ralchenko, V.; Karabutov, A.; Vlasov, I.; Frolov, V.; Konov, V.; Gordeev, S.; Zhukov, S.; Dementjev, A. Diamond–carbon nanocomposites: Applications for diamond film deposition and field electron emission. *Diam. Relat. Mater.* **1999**, *8*, 1496–1501. [CrossRef]

139. Karabutov, A.V.; Frolov, V.D.; Konov, V.I. Diamond/sp2-bonded carbon structures: Quantum well field electron emission? *Diam. Relat. Mater.* **2001**, *10*, 840–846. [CrossRef]

140. Zhu, W.; Kochanski, G.P.; Jin, S.; Seibles, L. Defect-enhanced electron field emission from chemical vapor deposited diamond. *J. Appl. Phys.* **1995**, *78*, 2707–2711. [CrossRef]

141. Geis, M.W.; Twichell, J.C.; Macaulay, J.; Okano, K. Electron field emission from diamond and other carbon materials after H_2, O_2, and Cs treatment. *Appl. Phys. Lett.* **1995**, *67*, 1328–1330. [CrossRef]

142. Takeuchi, D.; Koizumi, S.; Makino, T.; Kato, H.; Ogura, M.; Ohashi, H.; Okushi, H.; Yamasaki, S. Negative electron affinity of diamond and its application to high voltage vacuum power switches: NEA of diamond and its application to a high voltage vacuum power switch. *Phys. Status Solidi A* **2013**, *210*, 1961–1975. [CrossRef]

143. Takeuchi, D.; Nebel, C.E.; Yamasaki, S. Photoelectron emission from diamond. *Phys. Status Solidi A* **2006**, *203*, 3100–3106. [CrossRef]

144. Takeuchi, D.; Ogura, M.; Ri, S.-G.; Kato, H.; Okushi, H.; Yamasaki, S. Electron emission suppression from hydrogen-terminated n-type diamond. *Diam. Relat. Mater.* **2008**, *17*, 986–988. [CrossRef]

145. Takeuchi, D.; Nebel, C.E.; Yamasaki, S. Photoelectron emission properties of hydrogen terminated intrinsic diamond. *J. Appl. Phys.* **2006**, *99*, 086102. [CrossRef]

146. Takeuchi, D.; Kato, H.; Ri, G.S.; Yamada, T.; Vinod, P.R.; Hwang, D.; Nebel, C.E.; Okushi, H.; Yamasaki, S. Direct observation of negative electron affinity in hydrogen-terminated diamond surfaces. *Appl. Phys. Lett.* **2005**, *86*, 152103. [CrossRef]

147. Koizumi, S. Ultraviolet Emission from a Diamond pn Junction. *Science* **2001**, *292*, 1899–1901. [CrossRef] [PubMed]

148. Kono, S.; Koizumi, S. Images and Energy Distributions of Electrons Emitted from a Diamond pn-Junction Diode. *e-J. Surf. Sci. Nanotechnol.* **2009**, *7*, 660–664. [CrossRef]

149. Novoselov, K.S. Electric Field Effect in Atomically Thin Carbon Films. *Science* **2004**, *306*, 666–669. [CrossRef] [PubMed]

150. Di Bartolomeo, A.; Giubileo, F.; Romeo, F.; Sabatino, P.; Carapella, G.; Iemmo, L.; Schroeder, T.; Lupina, G. Graphene field effect transistors with niobium contacts and asymmetric transfer characteristics. *Nanotechnology* **2015**, *26*, 475202. [CrossRef] [PubMed]

151. Giubileo, F.; Di Bartolomeo, A. The role of contact resistance in graphene field-effect devices. *Prog. Surf. Sci.* **2017**, *92*, 143–175. [CrossRef]

152. Di Bartolomeo, A.; Giubileo, F.; Iemmo, L.; Romeo, F.; Santandrea, S.; Gambardella, U. Transfer characteristics and contact resistance in Ni- and Ti-contacted graphene-based field-effect transistors. *J. Phys. Condens. Matter* **2013**, *25*, 155303. [CrossRef] [PubMed]

153. Di Bartolomeo, A.; Giubileo, F.; Luongo, G.; Iemmo, L.; Martucciello, N.; Niu, G.; Fraschke, M.; Skibitzki, O.; Schroeder, T.; Lupina, G. Tunable Schottky barrier and high responsivity in graphene/Si-nanotip optoelectronic device. *2D Mater.* **2016**, *4*, 015024. [CrossRef]

154. Di Bartolomeo, A.; Luongo, G.; Giubileo, F.; Funicello, N.; Niu, G.; Schroeder, T.; Lisker, M.; Lupina, G. Hybrid graphene/silicon Schottky photodiode with intrinsic gating effect. *2D Mater.* **2017**, *4*, 025075. [CrossRef]

155. Vargas-Bernal, R. State-of-the-Art Electronic Devices Based on Graphene. In *Nanoelectronics and Materials Development*; Kar, A., Ed.; InTech: Rijeka, Croatia, 2016; ISBN 978-953-51-2525-9.

156. Giubileo, F.; Martucciello, N.; Di Bartolomeo, A. Focus on graphene and related materials. *Nanotechnology* **2017**, *28*, 410201. [CrossRef] [PubMed]

157. Lee, S.W.; Lee, S.S.; Yang, E.-H. A Study on Field Emission Characteristics of Planar Graphene Layers Obtained from a Highly Oriented Pyrolyzed Graphite Block. *Nanoscale Res. Lett.* **2009**, *4*, 1218–1221. [CrossRef] [PubMed]

158. Qian, M.; Feng, T.; Ding, H.; Lin, L.; Li, H.; Chen, Y.; Sun, Z. Electron field emission from screen-printed graphene films. *Nanotechnology* **2009**, *20*, 425702. [CrossRef] [PubMed]

159. Liu, J.; Zeng, B.; Wu, Z.; Zhu, J.; Liu, X. Improved field emission property of graphene paper by plasma treatment. *Appl. Phys. Lett.* **2010**, *97*, 033109. [CrossRef]

160. Xiao, Z.; She, J.; Deng, S.; Tang, Z.; Li, Z.; Lu, J.; Xu, N. Field Electron Emission Characteristics and Physical Mechanism of Individual Single-Layer Graphene. *ACS Nano* **2010**, *4*, 6332–6336. [CrossRef] [PubMed]

161. Xu, J.; Wang, Q.; Tao, Z.; Qi, Z.; Zhai, Y.; Wu, S.; Zhang, X.; Lei, W. Field Emission of Wet Transferred Suspended Graphene Fabricated on Interdigitated Electrodes. *ACS Appl. Mater. Interfaces* **2016**, *8*, 3295–3300. [CrossRef] [PubMed]

162. Eda, G.; Emrah Unalan, H.; Rupesinghe, N.; Amaratunga, G.A.J.; Chhowalla, M. Field emission from graphene based composite thin films. *Appl. Phys. Lett.* **2008**, *93*, 233502. [CrossRef]

163. Stratakis, E.; Eda, G.; Yamaguchi, H.; Kymakis, E.; Fotakis, C.; Chhowalla, M. Free-standing graphene on microstructured silicon vertices for enhanced field emission properties. *Nanoscale* **2012**, *4*, 3069. [CrossRef] [PubMed]

164. Malesevic, A.; Kemps, R.; Vanhulsel, A.; Chowdhury, M.P.; Volodin, A.; Van Haesendonck, C. Field emission from vertically aligned few-layer graphene. *J. Appl. Phys.* **2008**, *104*, 084301. [CrossRef]

165. Wu, Z.-S.; Pei, S.; Ren, W.; Tang, D.; Gao, L.; Liu, B.; Li, F.; Liu, C.; Cheng, H.-M. Field Emission of Single-Layer Graphene Films Prepared by Electrophoretic Deposition. *Adv. Mater.* **2009**, *21*, 1756–1760. [CrossRef]

166. Wang, K.; Feng, T.; Qian, M.; Ding, H.; Chen, Y.; Sun, Z. The field emission of vacuum filtered graphene films reduced by microwave. *Appl. Surf. Sci.* **2011**, *257*, 5808–5812. [CrossRef]

167. Pandey, S.; Rai, P.; Patole, S.; Gunes, F.; Kwon, G.-D.; Yoo, J.-B.; Nikolaev, P.; Arepalli, S. Improved electron field emission from morphologically disordered monolayer graphene. *Appl. Phys. Lett.* **2012**, *100*, 043104. [CrossRef]

168. Deng, J.; Zheng, R.; Yang, Y.; Zhao, Y.; Cheng, G. Excellent field emission characteristics from few-layer graphene–carbon nanotube hybrids synthesized using radio frequency hydrogen plasma sputtering deposition. *Carbon* **2012**, *50*, 4732–4737. [CrossRef]

169. Deng, J.; Zheng, R.; Zhao, Y.; Cheng, G. Vapor–Solid Growth of Few-Layer Graphene Using Radio Frequency Sputtering Deposition and Its Application on Field Emission. *ACS Nano* **2012**, *6*, 3727–3733. [CrossRef] [PubMed]

170. Ye, D.; Moussa, S.; Ferguson, J.D.; Baski, A.A.; El-Shall, M.S. Highly Efficient Electron Field Emission from Graphene Oxide Sheets Supported by Nickel Nanotip Arrays. *Nano Lett.* **2012**, *12*, 1265–1268. [CrossRef] [PubMed]

171. Lv, S.; Li, Z.; Liao, J.; Wang, G.; Li, M.; Miao, W. Optimizing Field Emission Properties of the Hybrid Structures of Graphene Stretched on Patterned and Size-controllable SiNWs. *Sci. Rep.* **2015**, *5*. [CrossRef] [PubMed]

172. Palnitkar, U.A.; Kashid, R.V.; More, M.A.; Joag, D.S.; Panchakarla, L.S.; Rao, C.N.R. Remarkably low turn-on field emission in undoped, nitrogen-doped, and boron-doped graphene. *Appl. Phys. Lett.* **2010**, *97*, 063102. [CrossRef]

173. Qi, J.L.; Wang, X.; Zheng, W.T.; Tian, H.W.; Hu, C.Q.; Peng, Y.S. Ar plasma treatment on few layer graphene sheets for enhancing their field emission properties. *J. Phys. D Appl. Phys.* **2010**, *43*, 055302. [CrossRef]

174. Wang, J.J.; Zhu, M.Y.; Outlaw, R.A.; Zhao, X.; Manos, D.M.; Holloway, B.C.; Mammana, V.P. Free-standing subnanometer graphite sheets. *Appl. Phys. Lett.* **2004**, *85*, 1265–1267. [CrossRef]

175. Panchakarla, L.S.; Subrahmanyam, K.S.; Saha, S.K.; Govindaraj, A.; Krishnamurthy, H.R.; Waghmare, U.V.; Rao, C.N.R. Synthesis, Structure, and Properties of Boron- and Nitrogen-Doped Graphene. *Adv. Mater.* **2009**, *21*, 4726–4730. [CrossRef]

176. Huang, C.-K.; Ou, Y.; Bie, Y.; Zhao, Q.; Yu, D. Well-aligned graphene arrays for field emission displays. *Appl. Phys. Lett.* **2011**, *98*, 263104. [CrossRef]

177. Lin, J.-C.; Huang, B.-R.; Lin, T.-C. Hybrid structure of graphene sheets/ZnO nanorods for enhancing electron field emission properties. *Appl. Surf. Sci.* **2014**, *289*, 384–387. [CrossRef]